Launcher Vehicle Aerothermodynamics and Fairing Separation Altitude Effects on Payload Temperature

Alessandro Falchi,[†] Lorenzo Gentile, Edmondo Minisci
Aerospace Centre of Excellence, University of Strathclyde
James Weir Building, 75 Montrose Street, Glasgow, G1 1XJ, UK
{alessandro.falchi, l.gentile, edmondo.minisci}@strath.ac.uk

Matteo Tirelli, Pierluigi Perugini

Avio SpA
Via Ariana, km 5.2, 00034 Colleferro (RM), Italy
{matteo.tirelli, pierluigi.perugini}@avio.com

Abstract

The first part of this research investigates and compares VEGA launcher vehicle aerothermodynamics during a nominal ascent trajectory simulated by means of Direct Simulation Monte Carlo and hypersonic local panel methods. In the second part of the work, the coupled aerothermal-structural simulation of the ascent phase up to 250s was performed, studying the heat transfer between the payload fairing and a dummy payload. The results have shown a good match among the aerothermal fluxes estimated by the different methodologies, and that an optimal theoretical fairing separation time can be found by minimizing the aerothermal fluxes incident on the payload.

1. Introduction

Hypersonic aerothermodynamics are of utmost importance in the design of launcher vehicles (LV). The sizing of thermal protection systems (TPS) is greatly affected by the outcome of computational and experimental measurements aiming at characterizing the aerothermal heating during the ascent phase, and such process influences directly the LV performances. The correct estimation of aerothermal fluxes and the associated uncertainties is important also when the temperature propagation within the internal structure of the LV. In fact, the aerothermal fluxes affect the internal equipment temperature prediction, determining whether or not they will remain within their operational temperature limits. The aerothermal heat fluxes are proven to be by far the highest contributors to the payload fairing (PLF) heating during the initial ascent phase, where the high density and hypersonic velocity causes extremely high convective heating. After the PLF separation, other heating sources, such as: albedo, sun, earth infrared radiation, and solid rocket motor (SRM) plume radiation have a relatively higher contribution.

The estimation of the hypersonic aerodynamics and aerothermodynamics of the LV is commonly performed via continuum computational fluid dynamics (CFD) methodologies, although such simulations present many difficulties and are computationally expensive. Indeed, during the ascent phase there are many variables that have to be taken into account, and creating aerodynamics and aerothermodynamics datasets for the various flight conditions requires to take into account different phenomena,[5,6,9] such as: SRMs plume interactions, variable atmospheric wind direction, different LV configurations (i.e.: stages separations), various geometric scales (i.e.: protrusions), and non-uniform wall temperature evolution.

In addition to such important factors, the atmospheric rarefaction degree over altitude changes of many order of magnitude, and around 100km the hypothesis of continuity on which common CFD methods are based begins to breakdown. The rarefaction degree is characterized by the Knudsen Number (Kn), which is defined as the mean free path to the object reference length ratio. At 100km, the typical Kn for a LV falls within the transitional rarefied regime (Kn within the interval from 0.1 to 10). Above 140km the flow falls within the free molecular regime, where the Kn is greater than 10), and the inter-molecular collisions become very rare and may be neglected. Within the transitional rarefied regime typical CFD methods do not provide accurate results, and different methods should be used to simulate the flow field around objects.[24]

LAUNCHER VEHICLE AEROTHERMODYNAMICS AND TEMPERATURE

The Direct Simulation Monte Carlo (DSMC) is applicable throughout all flow regimes, although its practical and efficient application found place mainly in both the transitional rarefied and free molecular regimes. The DSMC method solves the macroscopic flow field by simulating the inter-molecular collisions with a statistical approach, tracking the motion of the particles and computing the binary collisions.[3,4] Historically, the DSMC method has been used for characterizing various atmospheric re-entry scenarios,[33] studying hypersonic rarefied aerodynamics[13,31] and aerothermodynamics.[46] Different works provide a significant comparison of the aerodynamics and aerothermodynamics computed with both DSMC and typical CFD methods, for example: a thorough review and validation of DSMC applications has been published by Harvey,[17] a CFD-DSMC comparison within the quasi-rarefied transitional regime (Kn = 0.0019) of the Orion capsule aerothermodynamics was performed by Qian.[39] A complete study of the Apollo capsule aerothermodynamics ranging from the rarefied transitional regime (DSMC) to the continuum regime (Navier-Stokes equations) was presented by Moss.[32] The DSMC method has found its place for studying plume impingement and interactions with the free stream flow field of the Orion capsule.[25,38] Other interesting applications studies performed within rarefied conditions have been presented by Lebeau,[22] and among the different examples the surface pressure distribution of the Mir space station from the Space Shuttle jets during the docking, or the aerothermodynamics of missile defence systems along with the estimation of plume aerodynamics and surface heating.

The union of DSMC and CFD methods may provide a complete characterization of the aerothermodynamics with an excellent accuracy throughout the entire ascent phase of the LV, although their significant computational cost does not allow their use in a real-time coupling for simulating and propagating the ascent trajectory. In fact, each CFD or DSMC simulation may take hours and days running on high-performance computing clusters, whereas a step-by-step trajectory propagation may require several thousands of simulations making those high fidelity methods not suitable for the purpose. Such problem is often faced for studying the atmospheric re-entry of space debris, most commonly Low-Earth orbiting spacecraft at their end of life, or asteroids. Various software with different accuracy levels have been developed in the latest decades, for example: SCARAB,[21] Debris Assessment Software (DAS[35]), Debris Risk Assessment and Mitigation Analysis (DRAMA[16]). These software are based on low-fidelity hypersonic aerodynamics and aerothermodynamics, commonly known as local panel inclination (LPI) methods, and may provide a rapid estimation of the heat transfer on the re-entering object.

In the latest years, an open source LPI tool has been developed at the University of Strathclyde. The software initially presented as the Free and Open Source Tool for Re-entry of Asteroids and Debris[27] (FOSTRAD), and was tested on different geometries, such as the STS orbiter, CFASTT-1 space-plane and the Gravity field and steady-state Ocean Circulation Explorer satellite aerodynamics[2] (GOCE). FOSTRAD's aerodynamics module showed an acceptable accuracy with experimental data when studying blunt-shaped bodies,[26] but when applied to flat-shaped bodies like parallelepiped and flat cylinders the accuracy decreased. The software was progressively improved to allow a better aerodynamics and aerothermodynamics characterization of complex objects and spacecrafts. One of the most significant improvements was the introduction of a local radius-based approach on the standard LPI algorithm, which significantly increased the accuracy of the aerothermal heating estimation on complex objects.[12] Another significant update was the introduction of a coupling between the convective aerothermodynamics with a structural thermal and ablation code. Due to the shift in the application field, the software was later renamed as Spacecraft Tool for Re-entry and Aerothermal Analysis (STRATH-A). The upgraded software was tested on the Intermediate Experimental Vehicle (IXV), and the Stardust Sample Return Capsule (Stardust SRC); the analyses had shown a good approximation of high-fidelity aerothermal heat-fluxes distributions and provided a good match with both high fidelity simulations and experimental observations. Following the promising results, a validation campaign of the aerodynamic and aerothermodynamic modules of the developed tool was performed and will be published along with the official release of the developed open source code.[11]

The first part of this work focuses on the comparison of the early flight ascent phase (t < 250s) of the PLF convective aerothermal heating dataset (up to Kn = 0.5); DSMC analysis within the transitional and free molecular regime (down to Kn = 0.3, performed at the University of Strathclyde); and the aerothermal analysis performed with the low-fidelity tool STRATH-A throughtout the continuum, transitional, and free molecular regime. The simplified VEGA 3D model used for this work has been generated based on different sources which could be easily found in the internet.[1,15]

After the preliminary aerothermodynamics comparison, the software STRATH-A has been used to compute the PLF temperature during the LV ascent phase, simulating different PLF separation times ($T_{PLF,sep}$ = 200s, 215s, 231s) to evaluate its effects on a dummy payload (PL) external temperature, the respective simplified geometries have been reported in Figure 1. The temperature evolution has been studied introducing a 3D thermal model of both the PLF and dummy payload, assuming typical sun, albedo, earth environmental fluxes, and radiation toward the deep space.
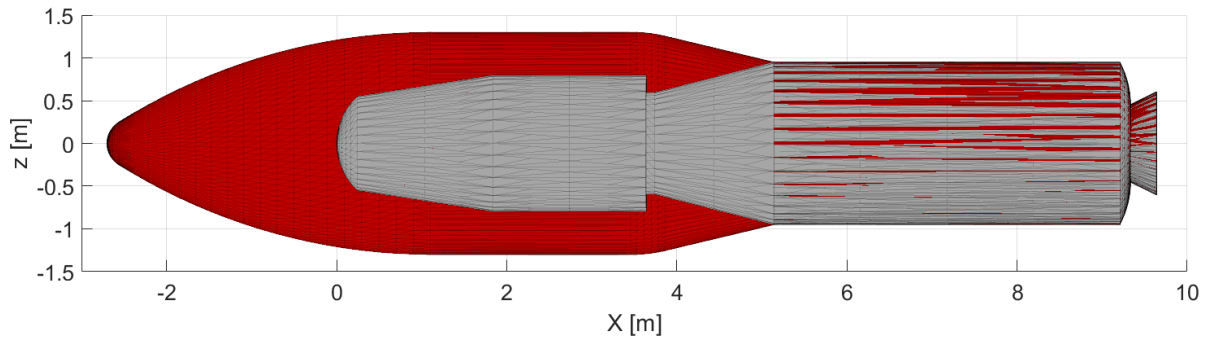
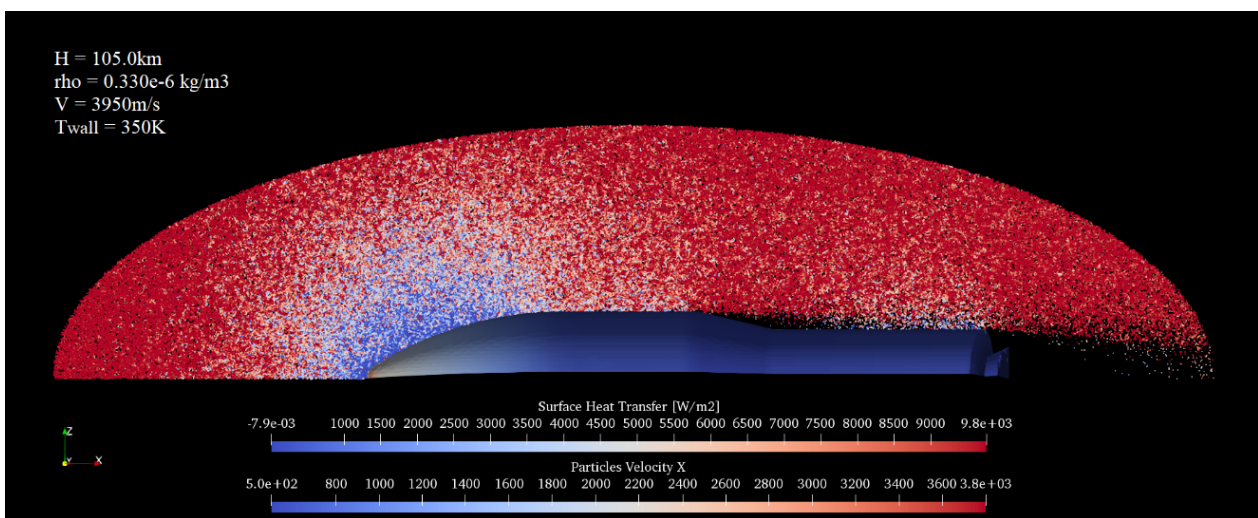Figure 1: Payload fairing, Z9 SRM, and dummy payload simplified geometric models

Figure 2: Payload Fairing and Z9 SRM simplified geometric model simulated at 105km, the particles velocity distribution and the surface heat transfer are reported in the two displayed color scales

2. Direct Simulation Monte Carlo

For performing the aerothermal analysis within the transitional regime, the dsmcFoam+[47] solver has been used. The software is based on the open source C++ platform OpenFOAM.[34] The solver was thoroughly validated in previous works, showing an excellent agreement with other DSMC solvers and experimental data.[41,42] The simulations have been performed with a non-reacting flow,[36] thus neglecting dissociation chemical reactions and thus computing an upper boundary for the surface heat transfer. The simulations have been performed with a diffusive wall boundary condition and a fixed wall temperature ($T_{wall} = 350K$). The molecular flow properties were obtained using a reference NRLMSISE-00 atmospheric dataset[37] based on a 5-species molecular mix (O, O_2, N, N_2, Ar). The altitude profile was chosen for a typical ascent trajectory publicly available in VEGA users manual.[1] The altitudes simulated with the DSMC method range between 105 and 130km, and fall within the ascent time interval from 195s to 240s, with a flight velocity around 3950m/s. The simulations required a preliminary convergence analysis on the cell size refinement, which has been conducted as the best practice suggests.[44] In figure 2, the post-processing of the simplified PLF geometrical model with Z9 (3rd SRM stage) has been shown. The figure shows the simulated particles velocity distribution (velocity on the +x direction) and the surface heat transfer at the altitude of 105km.

3. STRATH-A: Spacecraft Tool for Re-entry and Aero-Thermal Analysis

STRATH-A is the open source tool developed at the University of Strathclyde for performing low-fidelity hypersonic aerodynamic and aerothermodynamic analysis of complex objects. The tool is based on the local panel inclination methods, and has been continuously developed during the latest years aiming at providing preliminary and fast estimation of aerodynamic coefficients and heat transfer distributions throughout the atmospheric re-entry phase. The
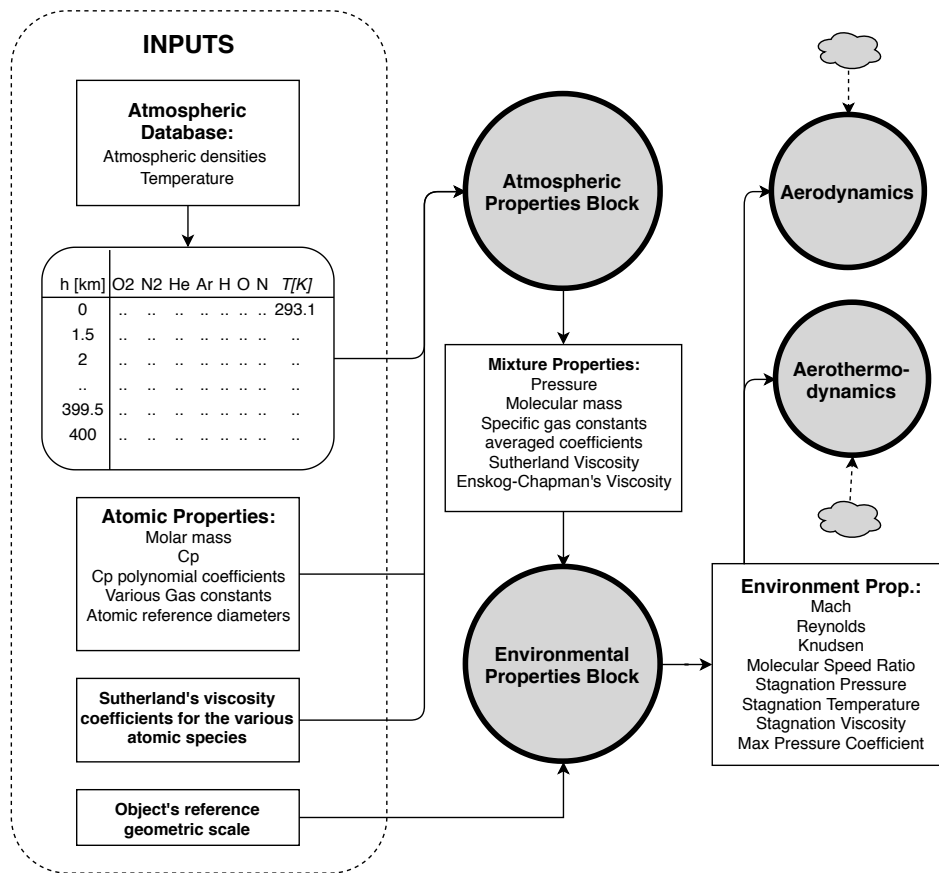
Figure 3: Atmospheric properties block structure, required an input atmospheric database, the geometric scale of the simulated object, the atmospheric properties constants (e.g.: viscosity coefficients, specific heats, molecular diameters)

tool has been validated and tested on various geometries and atmospheric re-entry scenarios,[2, 11, 12, 27] showing a good quantitative and qualitative match with both computational data (CFD, DSMC) and experimental observations.

STRATH-A has been developed with a modular structure, and in order to compute the aerothermodynamics of an object, it is required to first compute the atmospheric properties (Figure 3). After the atmospheric properties and external flow initialization, it is required to pre-process the mesh and the geometrical properties, identify the visible panels, and compute the local radius; the work-flow diagram is reported in Figure 4. After the initialization operations, the aerothermodynamics can be computed, and their formulations are dependent on the flow rarefaction degree (based on Kn). In the continuum regime, the formulations are dependent on the panels-flow inclination and the local radius. In the transitional regime, the heat transfer is dependent on the local panel inclination and local radius, and a set of generalized bridging functions calibrated on a set of test cases.[12] In the Free Molecular (FM) regime the heat transfer is dependent on the inclination of the panels. The aerothermodynamics block work-flow is reported in Figure 5, and more details about the three different continuum and free molecular regime sub-block are provided hereinafter.

3.1 Aerothermodynamics: continuum regime

Early developed in 1956, Lester Lees[23] studied the laminar heat transfer over a blunt-nosed body for a typical hypersonic atmospheric re-entry scenario, providing a first approximation for studying the relative heat transfer distribution of a hemisphere; At the end of 1956 Kemp and Riddell[19] proposed an approximation for estimating the heat transfer at the nose of a blunt body. Later in 1957, Fay and Riddell[14] investigated the heat transfer at the stagnation point taking into account the effects of molecular recombination and diffusion, which combined with Lees' relative heat transfer distribution could allow the surface heat-transfer estimation over a blunt object re-entering the atmosphere. In light of this latest research, in 1957 Detra, Kemp and Riddell[7] published an update of their initial experimental approximation for estimating the nose heat transfer:

$$q_s = \frac{17600}{\sqrt{R_N}} \sqrt{\frac{\rho_\infty}{\rho_{SL}}} \left(\frac{V_\infty}{V_{circ}}\right)^{3.15} \left(\frac{h_s - h_w}{h_s - h_{w,300}}\right) \qquad \left[\frac{Btu}{ft^2 s}\right] \qquad (1)$$
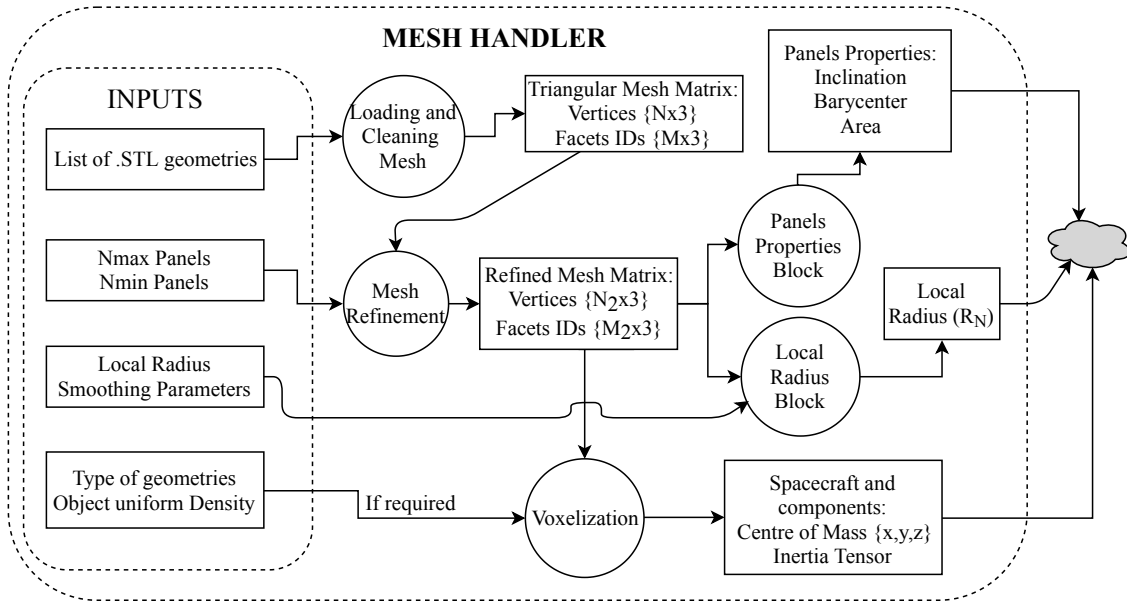
LAUNCHER VEHICLE AEROTHERMODYNAMICS AND TEMPERATURE

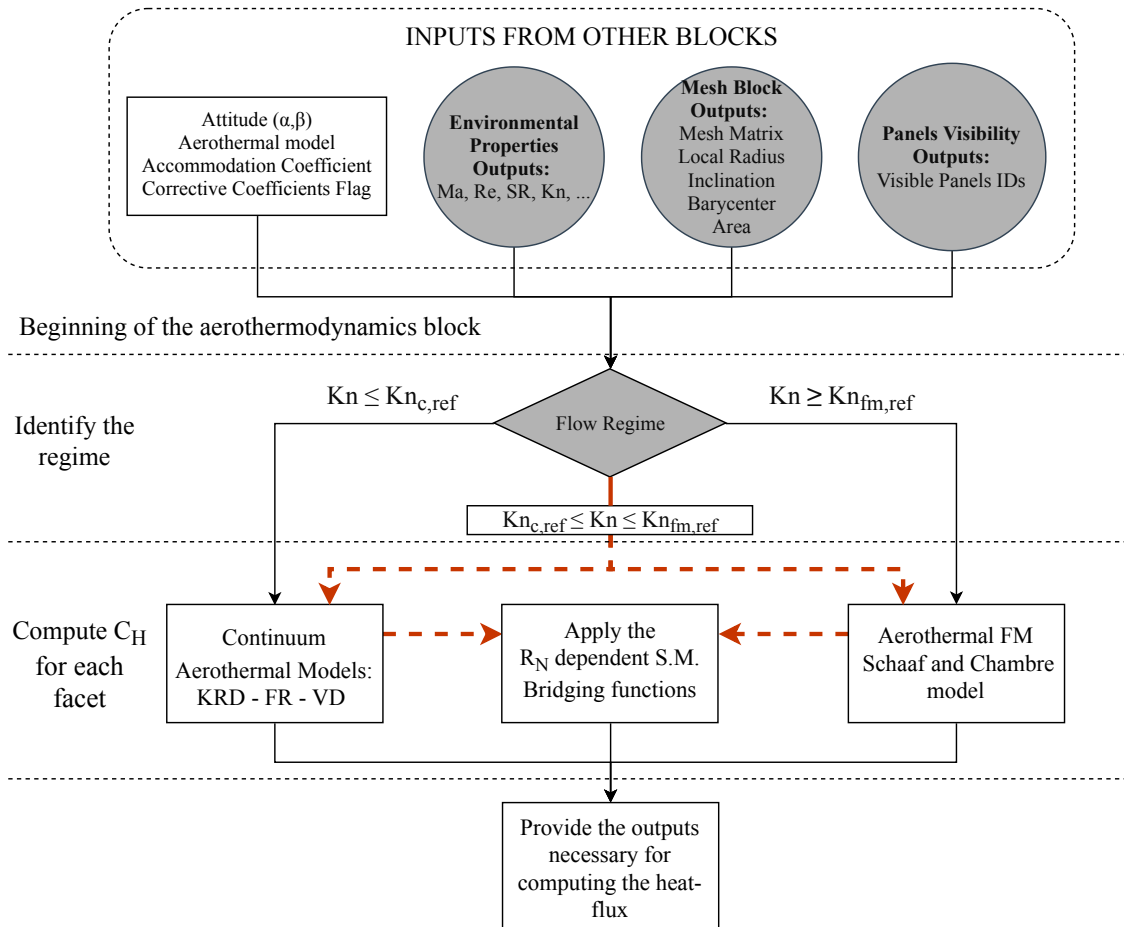Figure 4: Mesh handler block for performing the geometry initialization

Figure 5: Aerothermodynamics block work-flow diagram

where R_N is the nose radius, ρ_∞ and ρ_{SL} are the free flow and sea level mass densities, V_∞ and V_{circ} are the object relative velocity and the reference circular orbit velocity at the specific altitude, h is the enthalpy and the subscripts s,w represent the stagnation point and wall enthalpy respectively, and "w,300" represents the cold wall enthalpy (at 300K). Kemp-Rose-Detra (KRD) correlation was found to be valid between the sea level and 76km, and velocities between 2000m/s and 7600m/s with an error of ±10% with experimental observation, such approximation appears to be super catalytic if compared to Fay-Riddell fully catalytic model implementation. In 1959, Kemp et al.[20] proposed a more complex formulation taking into account also the flow local expansion ratio; based on the experimental data of a set of hypersonic shock-tubes experiments on a flat cylinder with rounded corners they proposed a new stagnation point heating relative distribution:

$$\frac{q}{q_s} = cos\left(\frac{\theta}{2}\right)^{5.27} \tag{2}$$

where q and q_s are the local heat transfer and the stagnation heat transfer respectively, while θ is the local flow inclination. Different extensions of these local inclination theories exist, for example Detra and Hidalgo[8] provided a characterization of the heat transfer in a turbulent flow, based on a running length correlation and a function of the local pressure ratio.

During the development of STATH-A, many different analyses were performed, one of the most significant was on the shock-tube experiments reported by Kemp et al.[20] Comparing the LPI simulations with experimental results, it appeared evident that the methodology should have been applied with a local radius, instead of using an effective reference radius. The local radius may be correlated with the flow local expansion ratio, which was quantitatively described by Kemp et al. For this reason a local radius smoothing algorithm was developed and introduced in STRATH-A. The algorithm was tested and calibrated on a set of reference geometries,[12] showing a good qualitative and quantitative agreement with different test cases.

3.2 Aerothermodynamics: free molecular regime

In the FM regime, the heat transfer can be computed assuming that the object does not influence the external flow field. For Kn greater than 10, the flow is generally considered to be "collisionless", and the flow velocity can be assumed to be equal to the Maxwellian distribution (dependent on the flow temperature) with a superimposed spacecraft relative velocity. The energy exchange with the object surface is largely dependent on the molecular diffusive accommodation coefficient, which depends on the re-emission of impacting molecules upon the surface, which can be diffusive or reflective. The diffusive accommodation coefficient is defined as:[30]

$$\sigma_{diff} = \frac{E_i - E_r}{E_i - E_w} \tag{3}$$

where σ_{diff} is the energy accommodation coefficient. E_i and E_r are the energy per unit area per second of the incident and re-emitted molecules respectively, E_w is the energy associated with re-emitted molecules at having a Maxwellian velocity probability distribution at the body wall temperature (T_w). Schaaf and Chambre[43] proposed a theoretical formulation for the heat flow of a flat plate dependent on the inclination angle, which assuming the following hypotheses:

- Steady state: number of impinging and re-emitted molecules is the same
- Re-emitted have a Maxwellian velocity dependent on T_w
- Perfect gas: internal degrees of freedom $j_{int} = (5 - 3\gamma)/(\gamma - 1)$ (where γ is the specific heat ratio)

can be defined as:[18]

$$
\begin{aligned}
q_{fm} \quad = \quad & \sigma_{diff} p_\infty \sqrt{\frac{RT_\infty}{2\pi}} \left\{ \left[S_R^2 + \frac{\gamma}{\gamma - 1} - \frac{\gamma + 1}{2(\gamma - 1)} \frac{T_w}{T_\infty} \right] \right. \\
& \left. \left[e^{-(S_R \sin\theta)^2} + \sqrt{\pi}(S_R \sin\theta)\left[1 + erf(S_R \sin\theta)\right] \right] - \frac{1}{2} e^{-(S_R \sin\theta)^2} \right\}
\end{aligned}
\tag{4}
$$

where q_{fm} is the heat transfer rate, p_∞ is the free flow pressure, R is the specific gas constant, T_w and T_∞ are the wall and free flow temperature respectively, θ is the panel inclination angle, γ is the specic heat ratio, $erf()$ is the typical error function, and S_R is the molecular speed ratio defined as:

$$S_R = \frac{V_\infty}{\sqrt{2RT_\infty}} \tag{5}$$

applying these equations the convective heat-flux on the inclined panels discretizing a complex object may be estimated, allowing the characterization of the heat flux distribution on complex bodies.
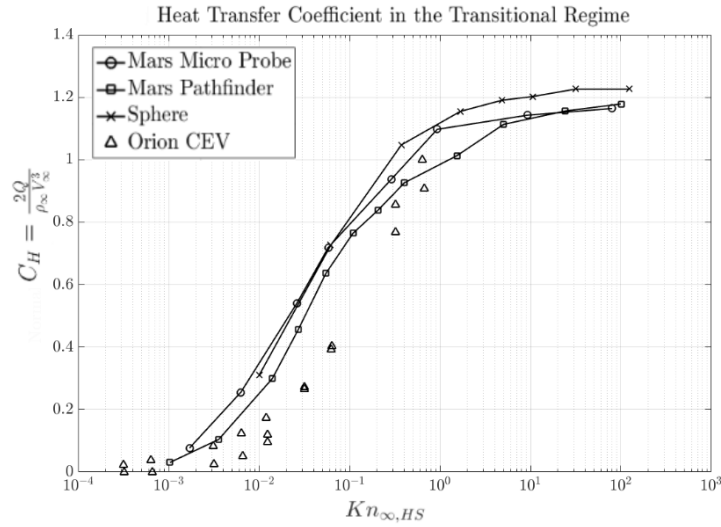
Figure 6: Heat transfer coefficients for various atmospheric re-entries of objects with different reference nose radius

3.3 Aerothermodynamics: transitional bridging functions

The characterization of the heat transfer within the transitional regime (i.e.: $0.1 \le Kn \le 10$) with LPI methods is most commonly performed via the application of object specific or generalized brdging functions.[21,40] In STRATH-A a set of generalized local radius-dependent bridging functions have been defined starting from a set of atmospheric re-entry reference data. In fact, by comparing the data from various re-entry scenarios, it was possible to observe how different reference nose radius influenced the qualitative shape of a possible bridging function. Some literature reference cases have been reported in Figure 6: Mars Microprobe[29] ($R_N = 0.0875m$), Mars Pathfinder[28] ($R_N = 0.664m$), a 1.6m diameter sphere simulated by Dogra[10] (extended in the upper FM regime with a set DSMC analyses), and Orion Crew Exploration Vehicle[27] ($R_N = 5.3m$).

4. Preliminary Aerothermodynamics Comparisons

One of the main objectives of this research was to run a set of simulations to compare STRATH-A aerothermal heat fluxes distributions against DSMC simulations at different altitude and flow conditions. The DSMC simulations have been performed with an average flow velocity of 3950m/s, and a fixed wall temperature of 350K with a diffusive wall boundary conditions. The atmospheric properties as a function of altitude have been reported in Table 1. The same conditions have been simulated with the STRATH-A low-fidelity tool, and the wall heat transfer distributions at the altitudes 105km, 107km, 110km, and 130km have been reported in Figures 7 and 8. The simulations with STRATH-A have been performed using the nose diameter as a reference length ($L_{ref} = 0.56m$) for computing the reference Knudsen number.

Table 1: DSMC atmospheric properties: altitude, temperature, mass density, and molecular density

H [km]	$T_\infty[K]$	$\rho_\infty[kg/m^3]$ $x10^{-9}$	$N_{He}[1/m^3]$ $x10^{12}$	N_O $x10^{15}$	N_{N_2} $x10^{15}$	N_{O_2} $x10^{15}$	N_{Ar} $x10^{15}$	N_H $x10^{12}$	N_N $x10^9$
105.0	210.8	340.28	154.8	537.7	5640.9	1132.9	51.3	21.8	393.6
107.2	231.6	232.44	142.9	450.2	3849.0	739.2	32.4	18.6	456.3
110.4	270.4	134.51	129.6	334.8	2222.1	398.0	16.6	14.5	567.5
115.4	340.5	53.14	97.3	178.0	872.9	140.1	5.4	8.2	687.9
120.0	409.9	24.74	74.4	101.6	403.8	58.7	2.1	4.8	828.3
125.2	483.1	13.11	61.2	64.1	212.0	27.7	1.0	3.0	1140.0
129.7	539.3	8.57	54.6	47.4	137.4	16.4	584.7	2.2	1583.0

One of the most significant sources of uncertainty in the computation of the LPI aerothermal heat transfer in the transitional regime is due to the reference length used for computing the Knudsen number. In fact, the transitional

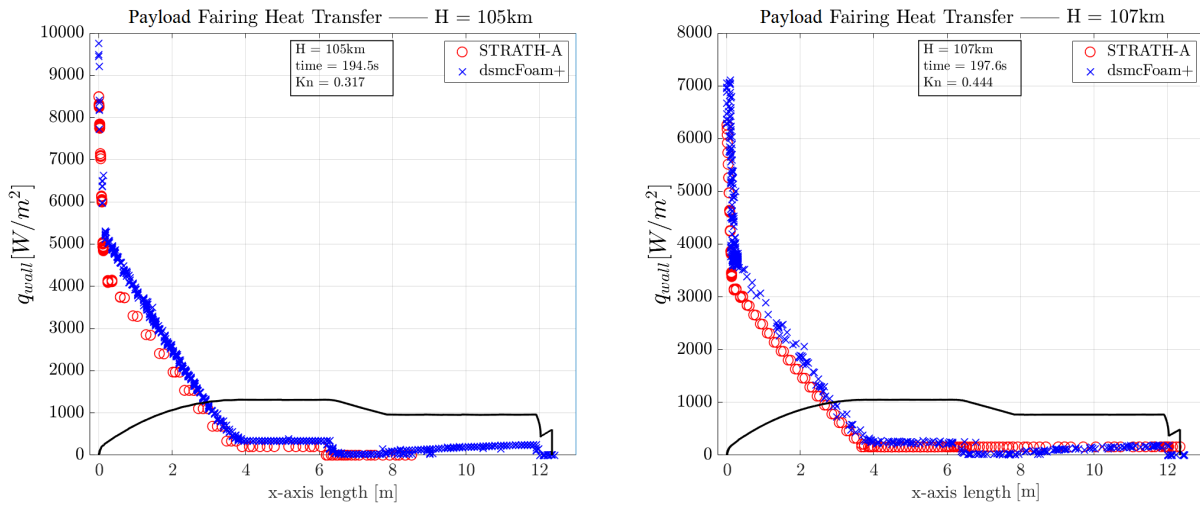LAUNCHER VEHICLE AEROTHERMODYNAMICS AND TEMPERATURE

Figure 7: Payload fairing Heat transfer distribution comparison between STRATH-A and dsmcFoam+ at 105km (on the left), and 107km (on the right)
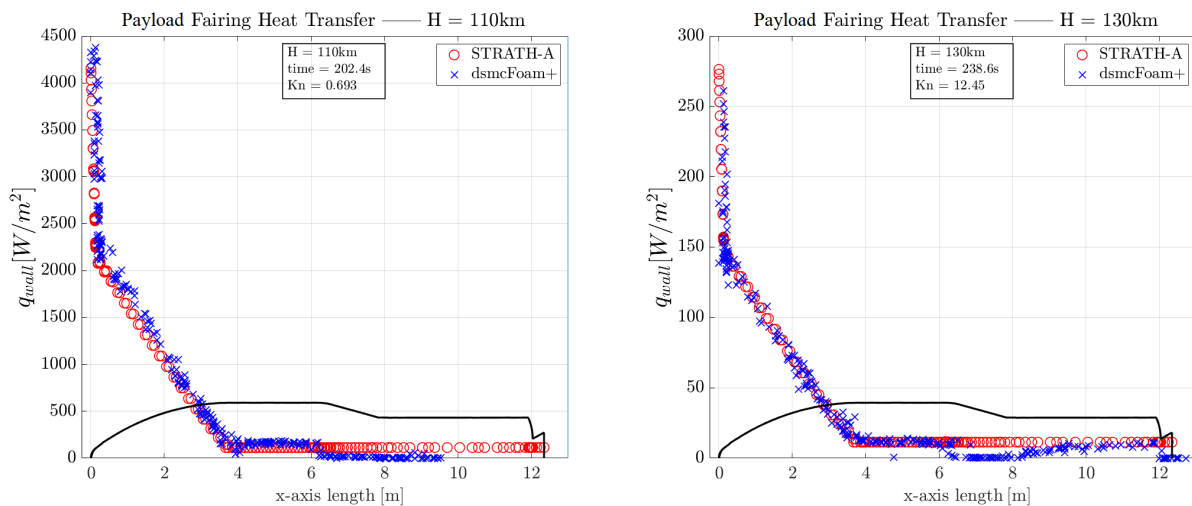
Figure 8: Payload fairing Heat transfer distribution comparison between STRATH-A and dsmcFoam+ at 110km (on the left), and 130km (on the right)
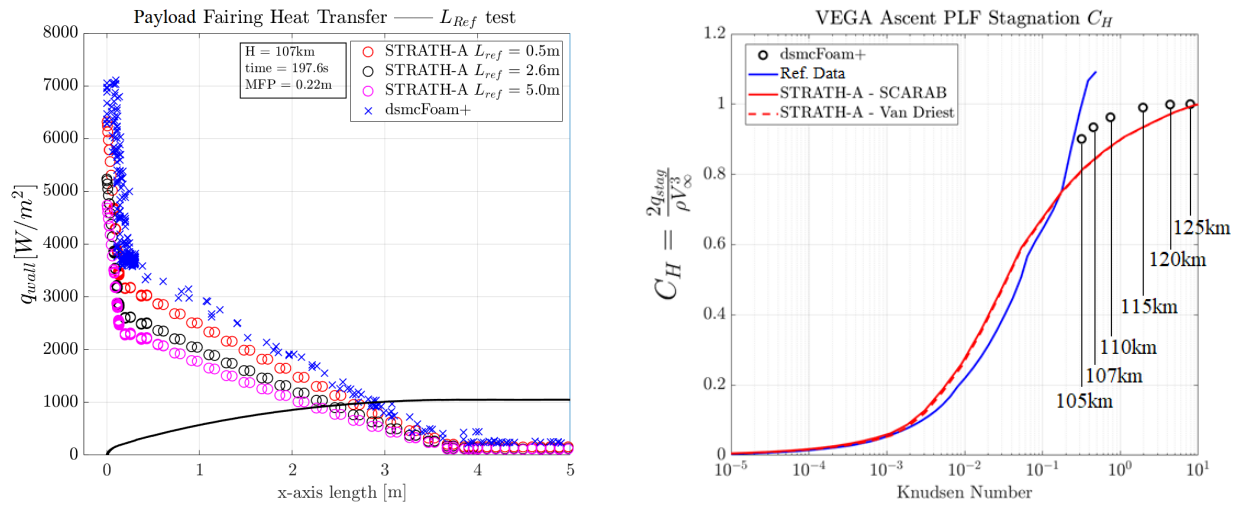
Figure 9: **On the left -** Sensitivity of the local heat transfer distribution on the reference length. **On the right -** comparison of the PLF nose heat transfer coefficient for a nominal VEGA trajectory

bridging function are characterized by a high uncertainty due to the limited number of data used to generate them, and therefore a small variation on the reference length is propagated to the estimated heat transfer. Three simulations were performed at the altitude of 107km using different reference lengths ($Lref = [0.5m, 2.6m, 5.0m]$, Figure 9 on the left). The PLF nose heat transfer computed with STRATH-A and dsmcFoam+ has been compared to a set of reference data of LV trajectories computed by means of CFD and LPI methods aiming at characterizing the heat transfer taking into account the uncertainties of a typical ascent scenario. The heat transfer coefficient over Kn has been reported in Figure 9 (on the right). The comparison between STATH-A and dsmcFoam+ show an excellent agreement on both the absolute heat transfer and the relative distribution; also the nose heat transfer coefficient show a good agreement among the different sources. Two different aerothermal formulation currently implemented in STRATH-A (for the continuum regime) have been compared: SCARAB[21] and Van Driest[45] which respectively compute an upper and lower boundary of the aerothermal heating; the results do not show an appreciable difference in the heat transfer coefficient linear scale, although the heat flux computed by the two formulations is sensibly different.

5. Application case: PLF and payload temperature estimation

The application case is focused on identifying a theoretical PLF separation time (or altitude) for a nominal VEGA ascent trajectory. Two different phases have been defined for performing the simulations: in the first one the PLF ascent was simulated, and its thermal model temperature was estimated, in the second phase, the internal heat radiated by the back-wall of the PLF was used as a boundary condition to estimated the dummy payload temperature.

5.1 PLF temperature estimation

In order to simulate the ascent scenario with STRATH-A, a coupled analysis between the aerothermal heat fluxes and a thermal model of the PLF had to be programmed. In Figure 10, the PLF thermal model schematic has been reported; the external thermal protection system (TPS) has been generated using 3 nodes through the thickness and 1 node to simulate the back-wall sandwich panel. The conductive links have been generated using a typical lumped thermal network approach. The specific model has been generated using approximately 10'000 nodes. Temperature-dependent properties (i.e.: thermal capacity and conductivity) have been used for both TPS and aluminum (sandwich). The internal radiation was neglected for simulating the ascent (the dummy payload was evaluated in a different uncoupled simulation), while the external surface has been assumed to be exposed to sun and albedo heat fluxes and an equivalent infrared Earth radiation. The external TPS infrared emissivity (ϵ) has been assumed equal to 0.9, while the solar absorptivity was assumed equal to 0.3.

The VEGA nominal ascent trajectory profile has been taken as an input from the user manual.[1] The trajectory was discretized in a sufficiently high number of steps; the PLF thermal model was coupled with the STRATH-A code to evaluate the aero-thermal heat fluxes to be used as boundary condition for each step. The internal convergence of
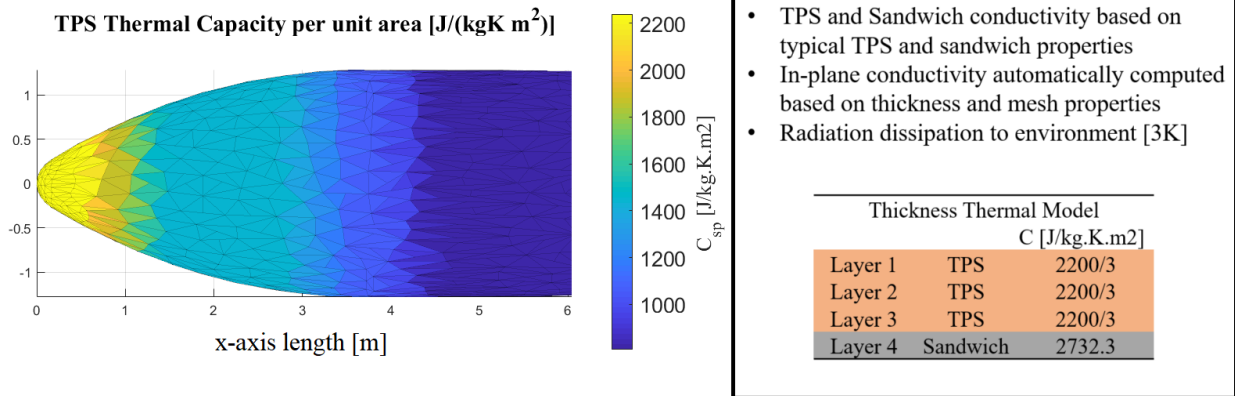
Figure 10: Payload fairing thermal model used to simulate the ascent trajectory, TPS and sandwich thermal capacities are based on typical values found in the literature
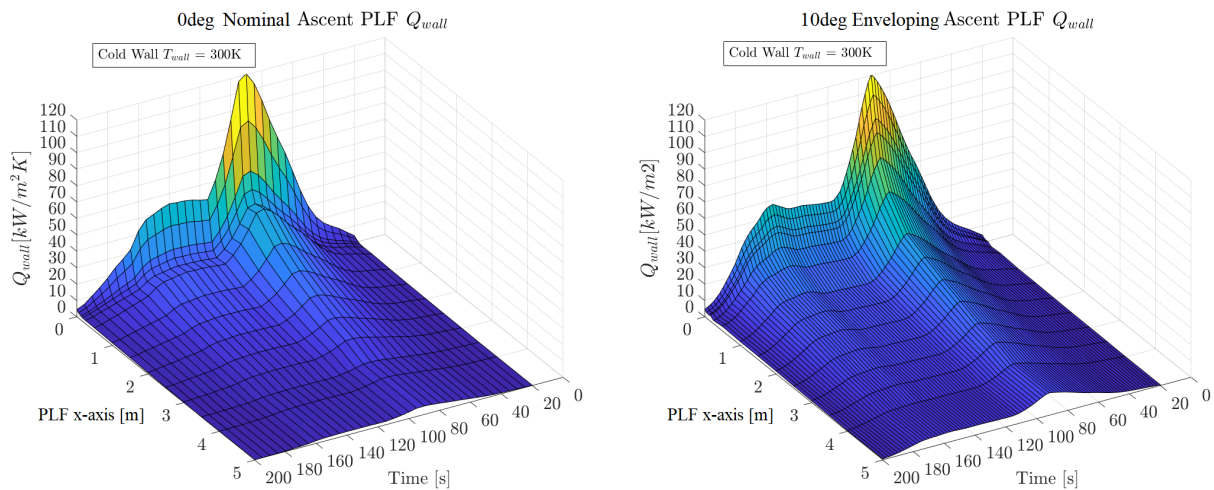

Figure 11: **On the left -** PLF heat transfer for the nominal ascent trajectory simulated with STRATH-A for AofA = 0deg. **On the right -** enveloping surface heat transfer for AofA = 10deg

the thermal model temperature was ensured using a variable time-step ODE solver (very high temperature gradients through the thickness and surface were expected).

The external TPS was simulated as a non-ablative material (such approach provides the highest back-wall temperature estimation). In order to apply an enveloping aerothermal heating, the simulations were performed assuming a reference angle of attack (AofA) of 10deg. Afterwards, the PLF length was discretized in 100 longitudinal stations, and the maximum aerothermal heating was computed and applied uniformly around the entire PLF circumference. In such a way, for the lower PLF longitudinal stations, a higher boundary aerothermal heating was applied. The 0deg and the enveloping 10deg angle of attack aerothermal heating distribution for a typical ascent trajectory over the PLF longitudinal axis are reported in Figure 11. The application of the enveloping Q_{wall} has been used as a boundary condition to simulate the PLF ascent. It may be observed that the reference heat fluxes have been computed assuming a cold wall (i.e.: $T_{wall} = 300K$), which is a conservative assumption for estimating the maximum aerothermal fluxes.

The results of the PLF ascent simulation for the wall temperature of the first TPS layer and the sandwich panel back-wall are reported in Figure 12. It is interesting to observe that the maximum back-wall temperature is not reached at the nose, but at the intersection between the ogive and the cylinder instead. Such result is due to the assumed progressively reducing TPS thermal capacity (and thickness) moving from the nose to the cylinder (Figure 10). Analyzing the results, and assuming a back-wall infrared emissivity equal to 0.85, the PLF internally emitted infrared radiation per unit area may be estimated with the Stefan-Boltzmann law. According to VEGA user manual,[1] the payload thermal environment requirement states that time-averaged or space-averaged internal PLF emitted radiation per unit area has to be lower than $1000W/m^2$ and the maximum transient value should be below $1300W/m^2$. In Figure 13, both the
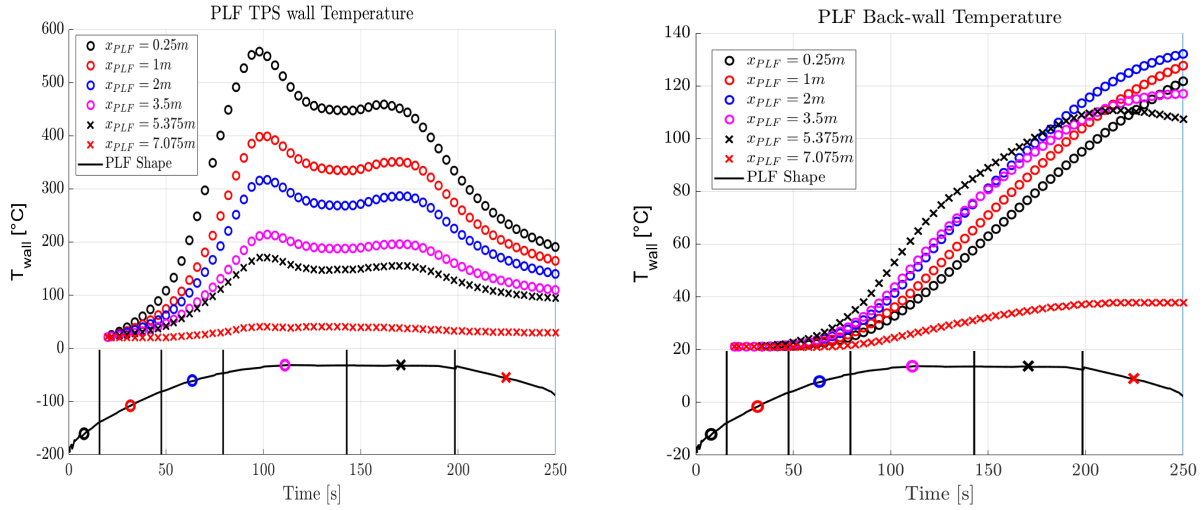
Figure 12: **On the left -** PLF averaged external TPS layer estimated wall temperature. **On the right -** PLF back-wall estimated temperature

emitted and the maximum absorbed radiative flux have been reported, the absorbed flux has been computed assuming a unitary view factor and the maximum back-wall temperature.

5.2 Dummy payload temperature estimation

The estimation of the dummy payload (PL) temperature has been performed assuming different boundary conditions depending on the PLF separation, and three different PLF separation times have been simulated: 200s, 215s and 231s (nominal separation time). The dummy payload has been simulated with a thermal model with 2 nodes through the thickness, using typical properties of sandwich panels and aluminum temperature-dependent properties (with an equivalent thermal capacity $C = 2950 J/kg.m^2.K$ per thickness node). In-plane and transverse conductivity have been assumed from equivalent sandwich panel properties. The PL infrared emissivity has been assumed equal to one, to estimate the maximum temperature increment for a given thermal capacity.

Before the PLF separation, only the back-wall radiative emitted heat flux is considered. At the front of the dummy payload (i.e.: rounded nose) the radiative links have been assumed with the PLF internal wall temperature estimated at $X_{PLF} = 2.0m$, while on the lateral surfaces the radiative link has been assumed with the PLF back-wall temperature at $X_{PLF} = 3.5m$ (see Figure 12 on the right). The radiative heat flux is computed as:

$$q_{rad,PL,i} = \sigma A_i V_{i,j} \epsilon_j \epsilon_i \left(T_{PLF,wall}^4 - T_{PL,i}^4 \right) \tag{6}$$

where $q_{rad,PL,i}$ is the net radiative flux absorbed by the external PL i-th node, A_i is the node surface, $V_{i,j}$ is the view factor which as been assumed equal to 1, ϵ is the correspondent infrared emissivity, $T_{PLF,wall}$ is the reference back-wall PLF temperature, and $T_{PL,i}$ is the PL i-th external panel temperature.

After the PLF separation, the aerothermal convective heat-flux is computed with STRATH-A, assuming the fluxes computed with a cold wall temperature assumption and a 10deg AofA envelope. When the nominal Z9 ignition time is reached (i.e.: t = 226s) the plume heat-fluxes defined by the VEGA user manual are applied[1] (Figure 14), and typical sun and albedo environmental heat fluxes are applied.

The results of the three different simulations for evaluating the PLF separation time influence on the PL external temperature have been reported in Figures 15-16, where the PLF separation and Z9 ignition time are also reported as dashed vertical lines. The results show different features: at the lowest simulated separation time, the aerothermal have a high impact on the front wall temperature, while at the other stations it is possible to observe that environmental and plume heat-fluxes have a higher contribution. Comparing $T_{PLF,sep} = 215s$ and $T_{PLF,sep} = 231s$, the temperature difference on the PL at 250s is almost negligible. In addition, it is possible to observe that between 215s and 231s, the PLF emitted infrared radiation becomes significant on the lateral surface, causing a temperature increment higher than the one that the external aerothermal fluxes would have caused. To further investigate the relative heat fluxes, the aerothermal and the PLF emitted fluxes have been compared, and they have been reported in Figure 17. Comparing the external convective heat fluxes with the PLF emitted radiation, it is possible to deduce that the optimal PLF separation
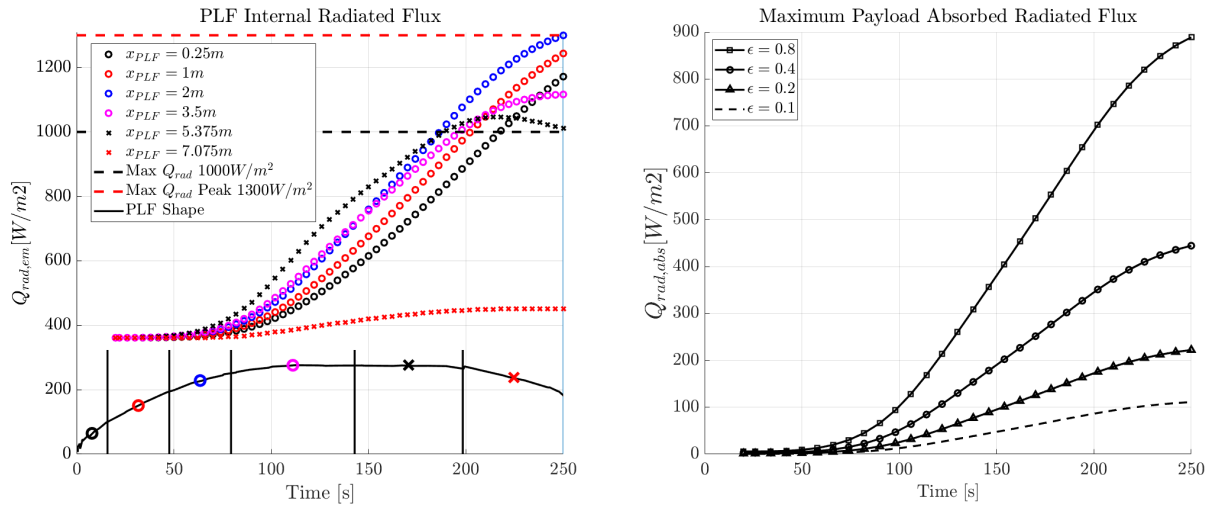
Figure 13: **On the left -** PLF internally emitted infrared radiation assuming $\epsilon = 0.85$ for the different averaged longitudinal stations. **On the right -** maximum radiative heat flux absorbed by the payload assuming an unitary view factor and four different infrared emissivity values
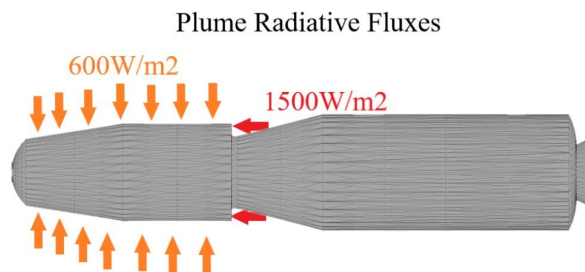

Figure 14: Z9 plume radiative heat fluxes as defined in VEGA user manual[1]
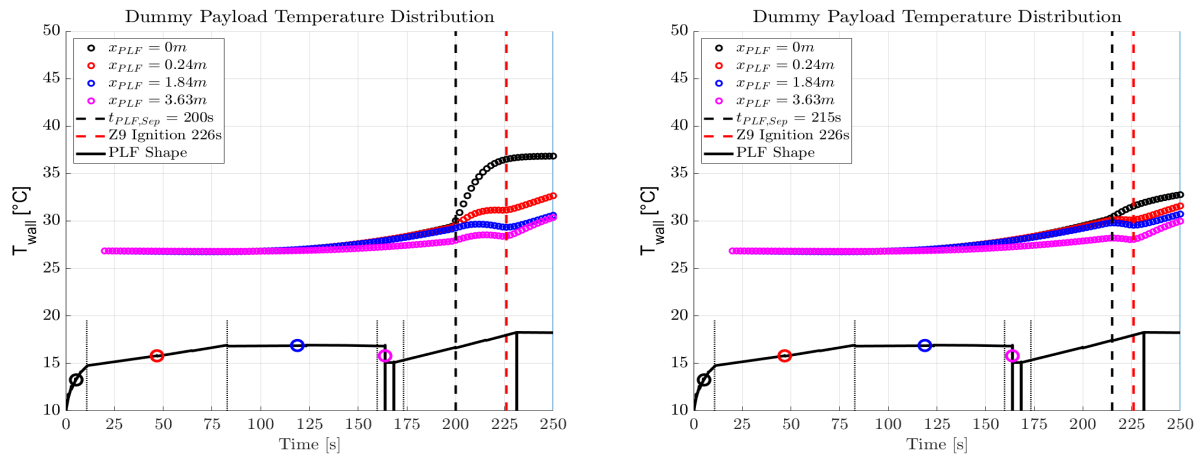
Figure 15: Dummy payload external wall averaged temperature predictions for different PLF separation times at different reference stations; on the left $T_{PLF,sep} = 200s$ and $T_{PLF,sep} = 215s$ on the right
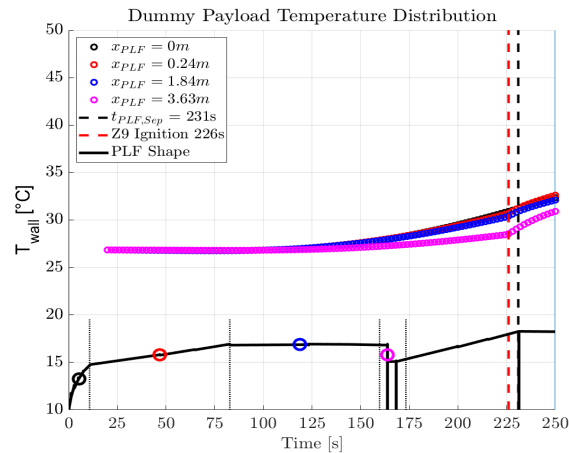

Figure 16: Dummy payload external wall averaged temperature predictions for different PLF separation times at different reference stations at the nominal $T_{PLF,sep} = 231s$

time would be at 214s. In addition, for the lateral payload stations, an earlier separation would be even more beneficial in order to minimize the incident heat-flux; such observation anchors the lateral stations higher wall temperature prediction reported by releasing the PLF at 231s (in Figure 16).

6. Conclusions

This research investigated the aerothermal heat fluxes on the geometrical shape of VEGA payload fairing, simulating the atmospheric flow condition occurring during a nominal ascent trajectory up to 250s. Initially, a preliminary comparison between high-fidelity DSMC simulation and a rapid local panel inclination software (STRATH-A) was performed. A limited number of altitudes with typical atmospheric properties and flight conditions of VEGA launcher vehicle were simulated (Table 1); the results have shown an excellent agreement within the rarefied transitional and free molecular regime (Figures 7-8). The results have also been compared to a set of reference nose cap heat transfer coefficients over a wide range of altitude (and Knudsen number), such comparison showed a good agreement between the bridging functions implemented within STRATH-A, the mixed CFD-LPI reference data, and the simulations performed with dsmcFoam+ (Figure 9, on the right).

After the initial comparison of the aerothermal heating, STRATH-A has been used to perform a coupled analysis of a simplified payload fairing (PLF) thermal model during the early ascent phase. After the initial PLF wall temperature estimation, the effect of the PLF time (and altitude) separation on a dummy payload temperature were investigated. The payload temperature prediction suggested that an early PLF separation would have been beneficial for reducing

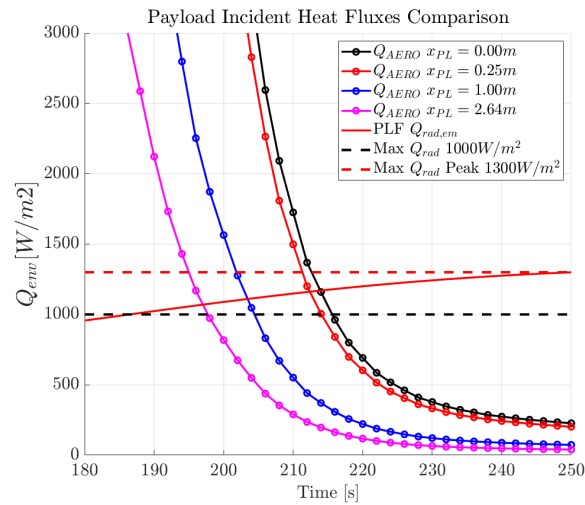LAUNCHER VEHICLE AEROTHERMODYNAMICS AND TEMPERATURE

Figure 17: Dummy payload potential external aerothermal convective fluxes and maximum PLF emitted radiative heat fluxes comparison at various reference stations

the averaged payload temperature (Figures 15-16).

Comparing the PLF internal radiated heat flux and the external aerothermal convective heat transfer of the reported simulations showed that an optimal theoretical PLF separation time may be found (Figure 17). Although it must be reminded that the simulations have been performed using literature-based thermal properties of TPS and sandwich materials, and not the actual thermal models of VEGA payload fairing.

In the simulated scenario, and the obtained results, a theoretical optimal separation was identified at 214s; such separation timing would allow to separate the payload between the Z23 separation and Z9 ignition. With respect to the nominal PLF separation time (231s), a cumulative Z9 firing time of 5 seconds could be performed without the weight of the PLF, allowing an overall increment of the LV performances.

The research highlighted the capability of the STRATH-A software to simulate ascent scenarios as well as re-entry scenario; thanks to the rapid estimation of aerodynamics and aerothermodynamics distribution such tool may be implemented in different fields, such as re-entry and ascent trajectory optimization, preliminary design for demise applications, thermal protection system preliminary design and sizing, and coupled trajectory propagation for statistical ground footprint estimation. The open source nature of the software would allow the integration and development by both industries and academic institutions, allowing to develop additional modules and allow the progressive development for research and system engineering purposes.

7. Acknowledgments

References

[1] Arianespace. Vega user's manual, issue 4, revision 0. *April*, 2014.

[2] G Benedetti, V Nicole, E Minisci, A Falchi, and M Vasile. Low-fidelity modelling for aerodynamic characteristics of re-entry objects. In - *To be published in the Proceedings of the Stardust Final Conference: Advances in Asteroids and Space Debris Engineering and Science, Springer*, 2016.

[3] GA Bird. Molecular gas dynamics and the direct simulation monte carlo of gas flows. *Clarendon, Oxford*, 508:128, 1994.

[4] Graeme Austin Bird. Molecular gas dynamics. *NASA STI/Recon Technical Report A*, 76, 1976.

[5] P Catalano, M Marini, A Nicoli, and A Pizzicaroli. Cfd contribution to the aerodynamic data set of the vega launcher. *Journal of Spacecraft and Rockets*, 44(1):42–51, 2007.

[6] Pietro Catalano, Marco Marini, Alessio Nicolì, and Antonio Pizzicaroli. Rans simulations of the flow past a launcher configuration in motor-on conditions. In *23rd AIAA Applied Aerodynamics Conference*, page 4964, 2005.

[7] RW Detra. Addendum to heat transfer to satellite vehicle reentering the atmosphere. *Jet Propulsion*, pages 1256–1257, 1957.

[8] RW Detra. Generalized heat transfer formulas and graphs for nose cone re-entry into the atmosphere. *ARS Journal*, 31(3):318–321, 1961.

[9] A Di Mascio, S Zaghi, R Muscari, R Broglia, B Favini, and A Scaccia. On the aerodynamic heating of vega launcher: Compressible chimera navier-stokes simulation with complex surfaces. In *7th European Aerothermodynamics Symposium, Brugge, Belgium*, pages 9–12, 2011.

[10] Virendra K Dogra, Richard G Wilmoth, and James N Moss. Aerothermodynamics of a 1.6-meter-diameter sphere in hypersonic rarefied flow. *AIAA journal*, 30(7):1789–1794, 1992.

[11] Alessandro Falchi. Atmospheric re-entry analysis of space objects. *PhD Thesis*, to be submitted.

[12] Alessandro Falchi, Viola Renato, Edmondo Minisci, and Massimiliano Vasile. Fostrad: An advanced open source tool for re-entry analysis. In *15th Reinventing Space Conference*, 2017.

[13] Jing Fan, Iain D Boyd, Chun-Pei Cai, Konstantinos Hennighausen, and Graham V Candler. Computation of rarefied gas flows around a naca 0012 airfoil. *AIAA journal*, 39(4):618–625, 2001.

[14] James A Fay. Theory of stagnation point heat transfer in dissociated air. *Journal of the Aerospace Sciences*, 25(2):73–85, 1958.

[15] frntr. Vega toy model rocket, 1999.

[16] Irene Pontijas Fuentes, Davide Bonetti, Federico Letterio, Gonzalo Vicario de Miguel, Gonzalo Blanco Arnao, Pedro Palomo, Cristina Parigini, Stijn Lemmens, Tobias Lips, and Ronny Kanzler. Upgrade of esa's debris risk assessment and mitigation analysis (drama) tool: Spacecraft entry survival analysis module. *Acta Astronautica*, 2017.

[17] John K Harvey. A review of a validation exercise on the use of the dsmc method to compute viscous/inviscid interactions in hypersonic flow. In *36 th AIAA Thermophysics Conference*, 2003.

[18] Wallace Hayes. *Hypersonic flow theory*. Elsevier, 1959.

[19] Nelson H Kemp and F. R. Riddel. Heat transfer to satellite vehicles re-entering the atmosphere. *Journal of Jet Propulsion*, 27(2):132–137, 1957.

[20] Nelson H Kemp, Peter H Rose, and Ralph W Detra. Laminar heat transfer around blunt bodies in dissociated air. *Journal of the aerospace sciences*, 26(7):421–430, 1959.

[21] G Koppenwallner, B Fritsche, T Lips, and H Klinkrad. Scarab-a multi-disciplinary code for destruction analysis of space-craft during re-entry. In *Fifth European Symposium on Aerothermodynamics for Space Vehicles*, volume 563, page 281, 2005.

[22] GJ LeBeau and FE Lumpkin Iii. Application highlights of the dsmc analysis code (dac) software for simulating rarefied flows. *Computer Methods in Applied Mechanics and Engineering*, 191(6-7):595–609, 2001.

[23] L Lees. Laminar heat transfer over blunt-nosed bodies at hypersonic flight speeds. *Journal of Jet Propulsion*, 26(4):259–269, 1956.

[24] Andrew J Lofthouse, Iain D Boyd, and Michael J Wright. Effects of continuum breakdown on hypersonic aerothermodynamics. *Physics of Fluids*, 19(2), 2007.

[25] J Marichalar, F Lumpkin, and K Boyles. Plume-free stream interaction heating effects during orion crew module reentry. 2012.

[26] P M Mehta, A Walker, M Brown, E Minisci, and M L Vasile. Sensitivity analysis towards probabilistic re-entry modeling of spacecraft and space debris. In *AIAA Modeling and Simulation Technologies Conference*, page 3098, 2015.

[27] Piyush Mehta, Edmondo Minisci, Massimiliano Vasile, Andrew C Walker, and Melrose Brown. An open source hypersonic aerodynamic and aerothermodynamic modelling tool. In *8th European Symposium on Aerothermodynamics for Space Vehicles*, 2015.

[28] Frank S Milos, Y-K Chen, William M Congdon, and Janine M Thornton. Mars pathfinder entry temperature data, aerothermal heating, and heatshield material response. *Journal of Spacecraft and Rockets*, 36(3):380–391, 1999.

[29] RA Mitcheltree, M DiFulvio, TJ Horvath, and RD Braun. Aerothermal heating predictions for mars microprobe. *Journal of spacecraft and rockets*, 36(3):405–411, 1999.

[30] K Moe, M M Moe, and S D Wallace. Improved satellite drag coefficient calculations from orbital measurements of energy accommodation. *Journal of spacecraft and rockets*, 35(3):266–272, 1998.

[31] James Moss, Katie Boyles, and Francis Greene. Orion aerodynamics for hypersonic free molecular to continuum conditions. In *14th AIAA/AHI Space Planes and Hypersonic Systems and Technologies Conference*, page 8081, 2006.

[32] James Moss, Christopher Glass, and Francis Greene. Dsmc simulations of apollo capsule aerodynamics for hypersonic rarefied conditions. In *9th AIAA/ASME Joint Thermophysics and Heat Transfer Conference*, page 3577, 2006.

[33] James N Moss and Graeme A Bird. Direct simulation of transitional flow for hypersonic reentry conditions. *Journal of spacecraft and rockets*, 40(5):830–843, 2003.

[34] OpenCFD Ltd. openFOAM Software Package, Ver. 2.3, Bracknell, England, U.K. `http://www.openfoam.com/`, 2016.

[35] J. N. Opiela, E. Hillary, D. O. Whitlock, and Hennigan M. Debris assessment software, user guide. Technical report, NASA Lyndon B. Johnson Space Center, January 2012.

[36] Rodrigo C Palharini, Craig White, Thomas J Scanlon, Richard E Brown, Matthew K Borg, and Jason M Reese. Benchmark numerical simulations of rarefied non-reacting gas flows using an open-source dsmc code. *Computers & Fluids*, 120:140–157, 2015.

[37] J. M. Picone, A. E. Heding, D. Pj. Drob, and A. C. Aikin. Nrlmsise00 empirical model of the atmosphere: Statistical comparisons and scientific issues. *Journal of Geophysical Research: space Physics*, 107(A12), 2002.

[38] Andrew Prisbell, J Marichalar, F Lumpkin, and G LeBeau. Analysis of plume impingement effects from orion crew service module dual reaction control system engine firings. In *AIP Conference Proceedings*, volume 1333, pages 595–600. AIP, 2011.

[39] Geng Qian and Bao-guo Wang. A comparative study of navier-stokes and dsmc simulation of hypersonic flowfields. In *49th AIAA Aerospace Sciences Meeting including the New Horizons Forum and Aerospace Exposition*, page 765, 2011.

[40] WC Rochelle, BS Kirk, and BC Ting. User's guide for object reentry analysis tool (orsat) version 5.0, vol. 1, jsc-28742, nasa lyndon b. *Johnson Space Center*, 1999.

[41] T. J. Scanlon, E. Roohi, C White, M. Darbandi, and J. M. Reese. An open source, parallel dsmc code for rarefied gas flows in arbitrary geometries. *Computers And Fluids*, 39(10):2078–2089, 2010.

[42] T J Scanlon, C White, M K Borg, R C Palharini, E Farbar, I D Boyd, J M Reese, and R E Brown. Open-source direct simulation monte carlo chemistry modeling for hypersonic flows. *AIAA Journal*, 53(6):1670–1680, 2015.

[43] Samuel Albert Schaaf and Paul L Chambré. *Flow of rarefied gases*. Number 8. Princeton University Press, 1961.

[44] Zhi-Xin Sun, Zhen Tang, Ya-Ling He, and Wen-Quan Tao. Proper cell dimension and number of particles per cell for dsmc. *Computers & Fluids*, 50(1):1–9, 2011.

[45] E Reginald Van Driest. *The problem of aerodynamic heating*. Institute of the Aeronautical Sciences, 1956.

[46] Raffaele Votta, Antonio Schettino, Giuliano Ranuzzi, and Salvatore FM Borrelli. Hypersonic low-density aerothermodynamics of orion-like exploration vehicle. *Journal of Spacecraft and Rockets*, 46(4):781–787, 2009.

[47] Craig White, Matthew K Borg, Thomas J Scanlon, Stephen M Longshaw, B John, DR Emerson, and Jason M Reese. dsmcfoam+: An openfoam based direct simulation monte carlo solver. *Computer Physics Communications*, 224:22–43, 2018.